15th Australasian Fluid Mechanics Conference
The University of Sydney, Sydney, Australia
13-17 December 2004

Experiments and Modeling of Impinging Jets and Premixed Stagnation Flames

J. M. Bergthorson[1], D. G. Goodwin[2], and P. E. Dimotakis[1]

[1]Graduate Aeronautical Laboratories
California Institute of Technology, Pasadena, CA, 91125, USA

[2] Department of Mechanical Engineering
California Institute of Technology, Pasadena, CA, 91125, USA

Abstract

Non-reacting impinging laminar jets and premixed methane-air flames are studied experimentally and numerically. Axial velocity measurements are performed using Particle Streak Velocimetry (PSV). The nozzle pressure drop is measured concurrently to determine the Bernoulli velocity. For cold impinging jets, scaling by the Bernoulli velocity collapses the centerline axial velocity profiles onto a single curve that is independent of the nozzle-plate separation distance. Cold-flow velocity profiles can be modeled using an error function with a single, Reynolds number dependent, parameter. Velocity data for cold impinging jets and premixed methane-air flames are compared to one-dimensional simulations with multi-component transport and full chemistry (GRI-Mech 3.0). Near-stoichiometric flames are studied as a function of the nozzle-stagnation plate separation distance. At constant Bernoulli velocity, flame profiles also collapse independently of separation distance. The results indicate that the one-dimensional streamfunction model can accurately capture both non-reacting and reacting stagnation flow if appropriate boundary conditions are specified.

Introduction

Premixed laminar flames offer a useful environment for validating chemical-kinetic mechanisms of hydrocarbon fuels. Studies that can be referenced to chemical kinetics over a variety of conditions (*e.g.*, equivalence ratio, ambient pressure, strain-rate field) are desirable. The approach here relies on detailed measurements of strained flames in a jet-wall stagnation flow. This geometry has boundary conditions that can be accurately specified, facilitating simulation and comparisons with experiment.

Velocity data for impinging jets in the nozzle-plate separation distance L to nozzle-diameter d ratio range of $0.5 \leq L/d \leq 1.5$ are not widely available. In addition, although stagnation flows have been employed in a large number of laminar flame studies, direct comparisons between flame measurements and simulations are sparse. When comparisons have been made, inlet velocity boundary conditions are treated as free parameters to align measured and simulated profiles (*e.g.*, [5]). This work targets the hydrodynamics of impinging jets and the effects of chemical reaction and the resulting heat release on this flow.

Velocity profiles are measured using Particle Streak Velocimetry (PSV) [1]. Concurrent measurements of the nozzle pressure drop are used to define the Bernoulli velocity U_B. Impinging jets are studied as a function of L at imposed strain rates (Reynolds numbers) of interest in laminar flame studies. Near-stoichiometric premixed methane-air flames are studied at constant U_B, as a function of L. One-dimensional (1D) simulations of cold and reacting stagnation flows are performed using *Cantera* to assess the streamfunction model employed [1, 2]. This work is part of an ongoing investigation into the performance of flow, transport and chemistry models for premixed hydrocarbon flames.

Experiments

A room-temperature, atmospheric-pressure jet is generated from a contoured nozzle with an exit diameter of $d = 10\,\mathrm{mm}$ that impinges on a constant-temperature (water-cooled) copper stagnation plate. Three K-type thermocouples are embedded on the centerline, spaced vertically between the stagnation and cooled surface, to allow monitoring of wall temperature and temperature gradients. Fuel and air mass flow rates are set using sonic metering valves and monitored concurrently (Omega FMA868-V-Methane and FMA872-V-Air, calibrated using a Bios DryCal ML-500). Estimated uncertainty in the mass-flow measurement of the air and fuel streams is 0.5%, resulting in an uncertainty of 0.7% in the equivalence ratio Φ.

The pressure difference between the jet plenum interior and a point just outside the jet-core flow region is measured with a 1 torr full-scale differential-pressure transducer (BOC Edwards W57401100 and W57011419). The Bernoulli velocity,

$$U_\mathrm{B} = \sqrt{\frac{2\,\Delta p}{\rho[1-(d/d_\mathrm{P})^4]}}\,, \qquad (1)$$

is then calculated, where Δp is the nozzle static pressure drop, ρ the fluid density, d the nozzle exit diameter, and d_P the plenum (inner) diameter. Pressure, mass-flow, and temperature data are acquired simultaneously with digital-image acquisition, allowing accurate specification of simulation boundary conditions.

Particle Streak Velocimetry (PSV)

Flow velocities along the jet centerline are measured using Particle Streak Velocimetry (PSV) [1]. The implemented PSV methodology yields low-fractional-error axial-velocity data, while requiring a low particle-seed density. Low particle loading reduces flame disturbances. A single PSV image can capture the entire velocity field, making it ideal for short-run-time experiments. A sample PSV image for impinging-jet flow is shown in figure 1. The measurements rely on micron-sized alumina particles and ceramic microspheres.

A Coherent I-90 Ar^+ laser, operated at $2-3\,\mathrm{W}$, provides the PSV illumination source. Two cylindrical lenses generate a thin laser sheet ($\approx 200\,\mu\mathrm{m}$) in the field of view. An Oriel (Model 75155) chopper with a 50% duty-cycle wheel modulates the laser beam. The chopper wheel is placed at a laser-beam waist to minimize on-off/off-on transition times. Chopping frequencies are in the range, $1\,\mathrm{kHz} \leq \nu_\mathrm{c} \leq 2\,\mathrm{kHz}$, with ν_c optimized depending on flow velocity. PSV image data are recorded at 4 fps using the in-house-developed "Cassini" CCD [1]. Magnification ratios are close to 1:1 using a Nikon 105 mm, $f/2.8$ macro lens (with a 514.5 nm bandpass filter).

Local velocities, $u(x)$, are estimated from streak pairs as, $u(x) \cong \Delta X(x)/\Delta t$, yielding $u_\mathrm{I} = L_\mathrm{I}/\tau_\mathrm{c}$ and $u_\mathrm{II} = L_\mathrm{II}/\tau_\mathrm{c}$, where $\tau_\mathrm{c} = 1/\nu_\mathrm{c}$ (chopping period) and $L_\mathrm{I} = x_{2\mathrm{s}} - x_{1\mathrm{s}}$ and $L_\mathrm{II} = x_{2\mathrm{e}} - x_{1\mathrm{e}}$ are the distances from the start/end of one streak to the start/end of

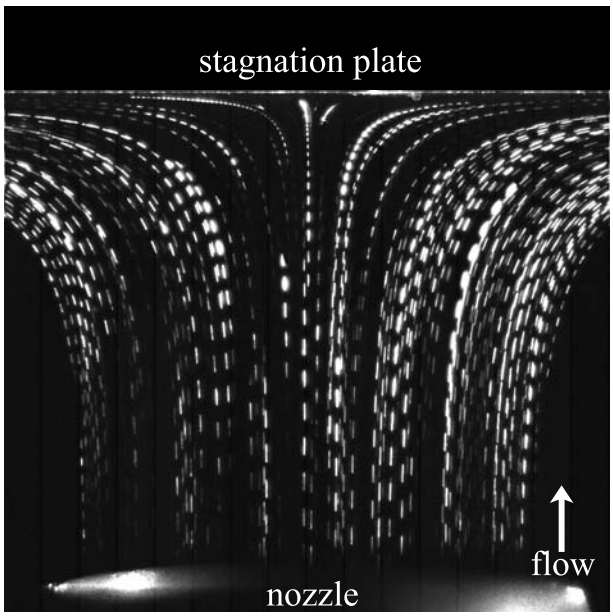

Figure 1: PSV in impinging-jet flow ($L/d = 1.0$).

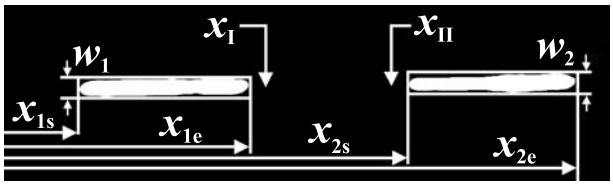

Figure 2: PSV measurement technique.

the next, respectively. The velocity estimate u_{I} is located at $x_{\mathrm{I}} = (x_{1\mathrm{s}} + x_{2\mathrm{s}})/2 + (w_1 + w_2)/4$, where $x_{i\mathrm{s}}$ is the spatial location of the start of the i^{th} streak and w_i is the width of the i^{th} streak. Similarly, u_{II} is located at $x_{\mathrm{II}} = (x_{1\mathrm{e}} + x_{2\mathrm{e}})/2 - (w_1 + w_2)/4$, where $x_{i\mathrm{e}}$ is the location of the end of the i^{th} streak (*cf*. figure 2). Using the same intensity threshold on a streak pair removes systematic errors in applying the Lagrangian time interval τ_{c} to the spatial extent of each streak. The PSV analysis technique yields an rms error of $\approx 0.01\,U_{\mathrm{B}}$. See [1] for additional details on PSV.

Simulations

Axisymmetric stagnation flow and premixed flame simulations are performed using the *Cantera* reacting-flow software package [1, 2]. The 1D model for stagnation flows relies on a stream-function $\psi(x,r) = r^2 U(x)$, with $U(x) = \rho u/2$, where u is the axial velocity. The momentum equation then becomes,

$$2U\frac{\mathrm{d}}{\mathrm{d}x}\left(\frac{1}{\rho}\frac{\mathrm{d}U}{\mathrm{d}x}\right) - \frac{1}{\rho}\left(\frac{\mathrm{d}U}{\mathrm{d}x}\right)^2 - \frac{\mathrm{d}}{\mathrm{d}x}\left[\mu\frac{\mathrm{d}}{\mathrm{d}x}\left(\frac{1}{\rho}\frac{\mathrm{d}U}{\mathrm{d}x}\right)\right] = \Lambda\,. \qquad (2)$$

In this formulation, $\Lambda \equiv (1/r)\,\mathrm{d}p/\mathrm{d}r$ and must be a constant. Treating Λ as unspecified, four boundary conditions are imposed on this third-order ordinary differential equation at $x = 0$ and $x = \ell$, with $0 < \ell \leq L$ a suitably chosen interior point, *e.g.*, $U(0) = 0$, $U'(0) = 0$, $U(\ell) = \rho_0\, u_\ell/2$, $U'(\ell) = \rho_0\, u'_\ell/2$, where ρ_0 is the density of the (cold) gas mixture, and u_ℓ and u'_ℓ are the velocity and velocity gradient at $x = \ell$. Energy and species equations are also solved with specification of inlet composition, inlet temperature, and stagnation-wall temperature boundary-conditions. The simulations use a multi-component transport model and the GRI-Mech 3.0 kinetics mechanism. A (multi-component) no-flux boundary condition for species is assumed at the wall.

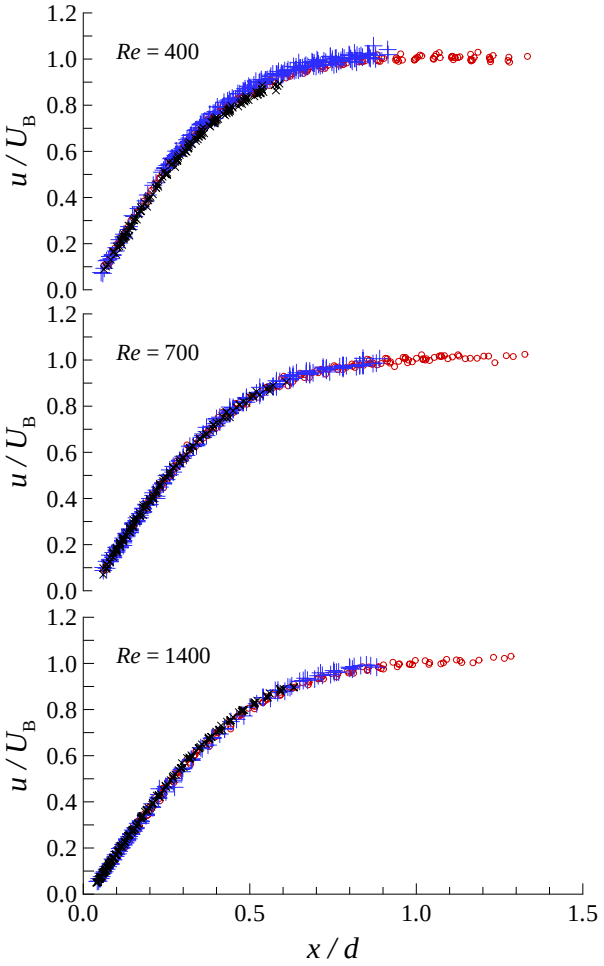

Figure 3: Comparison of velocity (scaled by U_{B}) versus axial distance from plate (scaled by d) at three nominal Reynolds numbers and $L/d = 1.4$ (○), 1.0 (+), and 0.7 (×).

Results

Cold impinging-jet velocity data are reported at three nominal Reynolds numbers, $Re \equiv \rho\, d\, U_{\mathrm{B}}/\mu \cong 400$, 700, and 1400, and three nozzle-to-stagnation plate separation distance to nozzle-diameter ratios, $L/d \cong 0.7$, 1.0, and 1.4. Figure 3 compares measured axial velocities, scaled by the Bernoulli velocity, for three L/d ratios at three Reynolds numbers. The velocity profiles collapse on a single curve, independent of L/d, if axial velocities are scaled by U_{B}. An axial velocity deficit at the jet-exit develops as the separation distance is decreased due to the influence of the stagnation point on the nozzle flow [6]. Notably, the velocity and its gradient adjust to maintain self-similarity, with the Bernoulli velocity scaling the flow.

In their study of cold turbulent jets, Kostiuk *et al*. [4] showed that opposed-jet or impinging-jet velocity data are well characterized by an error function. Their error function contained three adjustable parameters: the velocity at infinity U_∞, a strain-rate parameter α, and a wall-offset length δ/d,

$$u(x)/U_\infty \;=\; \mathrm{erf}\left[\alpha\,(x/d - \delta/d)\right]\,. \qquad (3)$$

Figure 3 indicates that an error function also characterizes laminar impinging-jet flow. The experimental data in figure 3 suggest that the appropriate velocity scale for laminar impinging jets is the Bernoulli velocity, *i.e.*, $U_\infty = U_{\mathrm{B}}$. From one-dimensional viscous stagnation-flow theory [7], the scaled-

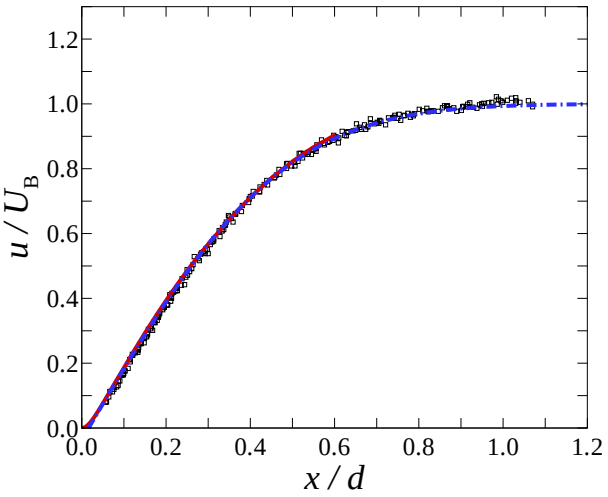

Figure 4: Cold-flow velocity profile corresponding to a $\Phi = 0.9$ methane-air flame ($Re = 1100$, $L/d = 1.2$). (□) exp. data, (solid red line) 1D simulation, (dot-dash blue line) error function.

Re	α	δ/d	ε_{rms}/U_B
400	2.21	0.027	0.017
700	2.00	0.020	0.010
1400	1.88	0.015	0.011

Table 1: Error-function fit parameters and resulting error ε_{rms}.

offset length δ/d, which is proportional to the wall-boundary-layer thickness, can be related to the strain-rate parameter α, such that, $\delta/d\,(Re,\alpha) = 0.7575\sqrt{1/(Re\,\alpha)}$. Thus, the only free parameter in this error-function is the Reynolds-number dependent strain-rate parameter $\alpha = \alpha(Re)$. The axial velocity field for an axisymmetric impinging laminar jet is then fully specified by the Bernoulli velocity U_B, since the Reynolds number, in turn, derives from it. The error function was fit to each experimental profile by adjusting α to minimize the root-mean-squared (rms) error ε_{rms}. For each Re, the strain-rate parameter α was averaged over the range $0.7 \le L/d \le 1.4$. This single $\alpha(Re)$ dependence was subsequently used in all error-function fits to determine the resulting rms error ε_{rms}. The fit parameters and ε_{rms} are shown in table 1.

Cold and reacting stagnation flows are studied for a near-stoichiometric, $\Phi = 0.9$, methane-air (CH_4-air) flame to determine the effect of heat release on the fluid mechanics and the ability of the one-dimensional simulations to capture the flow. The nozzle-stagnation plate separation distance L is varied at constant Φ to study the hydrodynamics at constant chemistry. Figure 4 shows the measured velocity data for a cold-flow at $Re \cong 1100$ and $L/d = 1.2$. Velocities are scaled by U_B and axial-distances by d. The error-function profile with $\alpha = 1.95$, interpolated for $Re = 1100$, is included and accurately models the flow. Exploiting the inviscid, constant-density solution to equation (2), which is a parabola, a quadratic is fit to the velocity profile in the range $0 \le x/d \le 0.8$. The values u_ℓ and u'_ℓ are calculated from the fit at $x = \ell$, with $U(\ell) = \rho_0\, u_\ell/2$ and $U'(\ell) = \rho_0\, u'_\ell/2$ then specifying the boundary conditions. In this work, ℓ/d is fixed at 0.6. As can be seen, the one-dimensional model accurately captures the flowfield if velocity boundary conditions are specified in this manner.

Figure 5 shows velocity profiles for a $\Phi = 0.9$ methane-air flame at $L/d = 1.2$ and $Re \cong 1100$. The cold-flow (error-function) profile is also included for comparison. Simulation boundary

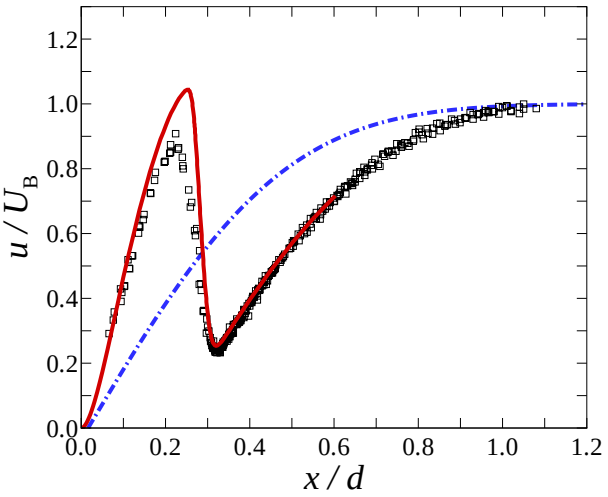

Figure 5: CH_4-air flame profiles ($\Phi = 0.9$, $L/d = 1.2$). (□) exp., (solid red line) 1D sim., (dot-dash blue line) error-function.

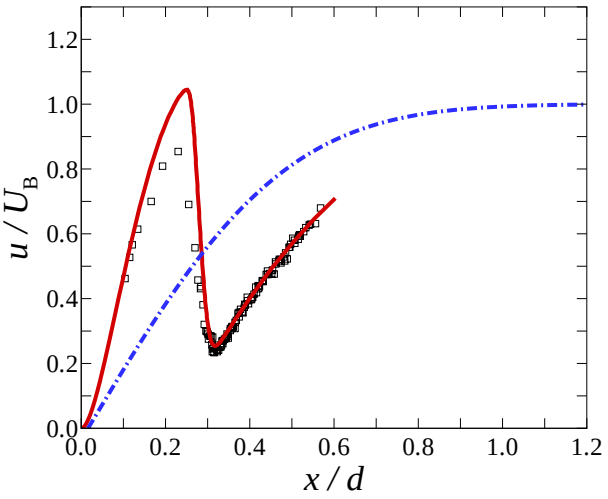

Figure 6: CH_4-air flame profiles ($\Phi = 0.9$, $L/d = 0.6$). Legend as in figure 5.

conditions are specified from a fit to the cold-flow portion of the profile ($0.35 < x/d < 0.80$) to determine u_ℓ and u'_ℓ. The simulated velocity profile is in good agreement with experiment, but predicts a higher post-flame velocity than measured. The PSV chopping frequency was optimized for the cold upstream region and not for this high-velocity, high-curvature region of the flow. While accounting for this brings experiment and simulation closer, it does not account for the difference. The flame produces a virtual stagnation point that alters the flowfield, although the strain rate, $\sigma = \mathrm{d}u/\mathrm{d}x$, upstream of the flame is very close to that of the cold flow. Figure 6 depicts measured and simulated velocity profiles for a $\Phi = 0.9$ methane-air flame at $L/d = 0.6$ and $Re \cong 1100$. Again, good agreement is seen except for an overprediction of post-flame velocities. A nozzle-exit-velocity deficit is evident compared to the cold flow.

A comparison of experimental velocity profiles at variable L/d and constant U_B is given in figure 7. The velocity profiles collapse on a single curve, independent of L/d, if the Bernoulli velocity is held constant. As all datasets were recorded for essentially the same flame, the agreement between experiment and simulation for $L/d = 0.8$ and 1.0 is consistent with that

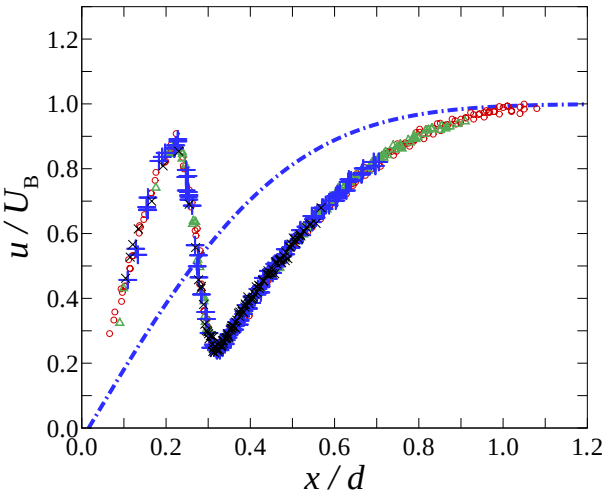

Figure 7: CH_4-air flame profiles ($\Phi = 0.9$) at: $L/d = 1.2$ ($\circ$), $L/d = 1.0$ ($\triangle$), $L/d = 0.8$ ($+$), and $L/d = 0.6$ ($\times$). Cold-flow error function is also included (dot-dash blue line).

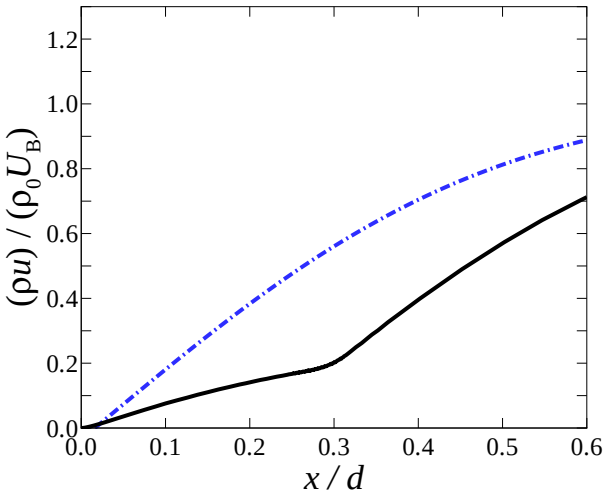

Figure 8: Simulated CH_4-air flame profile of ρu at $\Phi = 0.9$ (solid black line). Cold-flow error function (dot-dash blue line).

seen in figures 5 and 6. The imposed strain rate σ can be defined as the maximum slope of the velocity profile upstream of the flame. The strain rate for the flames presented in figure 7 is $\sigma \cong 360\text{s}^{-1}$. This is very close to the maximum strain rate for the cold-flow profile of $\sigma \cong 365\text{s}^{-1}$ (*cf*. figure 4). This flame is not close to extinction conditions, as verified experimentally and predicted numerically. The "global strain rate" has been defined as the nozzle-exit velocity divided by the nozzle-stagnation point separation distance (*e.g.*, [8]). For the flames studied here the global strain rate varies from 140s^{-1} at $L/d = 1.2$ to 190s^{-1} at $L/d = 0.6$. This indicates that the global strain rate, based on the centerline nozzle-exit velocity, does not provide a good surrogate for the strain rate imposed on the flame. However, Kobayashi and Kitano [3] found a good correlation between the global strain rate based on the mean nozzle-exit velocity and the velocity gradient upstream of the flame. This may be due to their different definition of global strain rate. Figure 8 plots the product of the simulated velocity and density profiles, scaled by the cold-flow density ρ_0 and U_B. The profile of ρu is composed of two stagnation flows with different gradients in the cold and hot regions of the flow.

Conclusions

Velocity profiles are measured, using PSV, in impinging jets and methane-air stagnation flames. For impinging jets, velocity profiles are found to collapse when scaled by the Bernoulli velocity. These profiles are well characterized by an error-function model in terms of a single, Reynolds number dependent, parameter. One-dimensional simulations can accurately capture the flow if the boundary conditions are correctly specified. Near-stoichiometric flames are studied as a function of the nozzle-stagnation plate separation distance. The flames are simulated using a one-dimensional model with multi-component transport and full chemistry (GRI-Mech 3.0). Good agreement is found between experiment and simulation. Flame velocity profiles collapse to a single curve at a fixed Bernoulli velocity, independent of the separation distance. The strain rate in the reacting flow is very close to that of the corresponding impinging jet. The results indicate that the global strain rate, based on the centerline nozzle-exit velocity, is not a good surrogate for the applied strain to the flame as it is dependent on the separation distance, while the maximum velocity gradient upstream of the flame is not. The profile of the product of the density and velocity indicates that the reacting flow is characterized by two stagnation flows with different gradients. Ongoing research targets the effect of the imposed strain rate on premixed hydrocarbon flames and the performance of transport and chemistry models.

Acknowledgements

We would like to acknowledge discussions with T. W. Mattner and K. Sone, as well as contributions by D. Lang to digital imaging, and G. Katzenstein to mechanical design. The work was funded by AFOSR Grant F49620–01–1–0006, whose support is gratefully acknowledged.

References

[1] Bergthorson, J. M., Goodwin, D. G. and Dimotakis, P. E., Particle streak velocimetry and CH laser-induced fluorescence diagnostics in strained, premixed, methane-air flames, *Proc. Combust. Inst.*, **30**, (in press).

[2] Goodwin, D. G., An open-source, extensible software suite for CVD process simulation, in *Proc. of CVD XVI and EuroCVD Fourteen*, Electrochem. Soc., 2003, 155–162.

[3] Kobayashi, H. and Kitano, M., Effects of equivalence ratio on the extinction stretch rate of cylindrical premixed flames, *Combust. Sci. Technol.*, **89**, 1993, 253–263.

[4] Kostiuk, L. W., Bray, K. N. C. and Cheng, R. K., Experimental study of premixed turbulent combustion in opposed streams: Part I - non-reacting flow field, *Combust. Flame*, **92**, 1993, 377–395.

[5] Law, C. K., Sung, C. J., Yu, G. and Axelbaum, R. L., On the structural sensitivity of purely strained planar premixed flames to strain rate variations, *Combust. Flame*, **98**, 1994, 139–154.

[6] Rolon, J. C., Veynante, D., Martin, J. P. and Durst, F., Counter jet stagnation flows, *Exp. Fluids*, **11**, 1991, 313–324.

[7] Schlichting, H., *Boundary layer theory*, McGraw-Hill Book Company, Inc., New York, 1960, 81–83.

[8] Zhang, H. and Egolfopoulos, F. N., Extinction of near-limit premixed flames in microgravity, *Proc. Combust. Inst.*, **28**, 2000, 1875–1882.